

# Indications of a Late-Time Transition to a Strongly Interacting Dark Sector

Andronikos Paliathanasis<sup>1, 2, 3, 4, \*</sup>

<sup>1</sup>*Institute of Systems Science, Durban University of Technology, Durban 4000, South Africa*

<sup>2</sup>*Centre for Space Research, North-West University, Potchefstroom 2520, South Africa*

<sup>3</sup>*Departamento de Matemáticas, Universidad Católica del Norte,*

*Avda. Angamos 0610, Casilla 1280 Antofagasta, Chile*

<sup>4</sup>*National Institute for Theoretical and Computational Sciences (NITheCS), South Africa.*

(Dated: January 7, 2026)

We explore the transition from the  $\Lambda$ CDM to an interacting dark sector by introducing a model with a redshift threshold that controls the onset of the energy transfer between the dark energy and the dark matter. Below the transition redshift, the interaction between dark matter and dark energy becomes active, while at earlier times the cosmological evolution coincides with that of  $\Lambda$ CDM. This approach allows us to determine the epoch in the cosmic history where the interacting effects have an impact in the description of the dark sector. We constrain the free parameters of the model using late-time cosmological observations, namely Cosmic Chronometers, DESI DR2 Baryonic Acoustic Oscillations, and Supernova data from the Pantheon Plus, Union3.0, and DES-Dovekie catalogues. The analysis provides an indication of a strong interacting term that describes energy transfer from dark energy to dark matter, which is activated at low redshifts. The PantheonPlus sample provides a threshold of  $z_T < 0.624$ , the Union3.0 sample yields  $z_T = 0.400^{+0.021}_{-0.23}$ , and the DES-Dovekie sample gives  $z_T = 0.371^{+0.028}_{-0.26}$ . The model fits the data in a similar way to the CPL parametrization, without the dark energy to cross the phantom divide line.

Keywords: Cosmological Constraints; Interacting Dark Sector; Dark Energy

## 1. INTRODUCTION

The second data release of Baryon Acoustic Oscillation (BAO) measurements from the Dark Energy Spectroscopic Instrument (DESI DR2) [1–3] provides support for cosmological scenarios in which dark energy has a dynamical character [4–12]. These findings are consistent with earlier indications obtained from previous data sets [13–18].

The origin and nature of the dark energy is unknown; nevertheless there are various approaches in the literature which investigate the dynamical behaviour of the dark energy, see for instance [19–50] and references therein.

Interacting dark sector models have received high attention recently [51–69]. In such models, dark energy and dark matter form the dark sector of the universe. While the total dark sector is conserved, the individual components are not, indicating the presence of an energy exchange between the elements of the dark sector. In interacting models dark energy and dark matter can be seen as two representations of the total cosmic fluid, and the energy transfer is analogue to a phase transition.

Cosmological models with dark energy-dark matter interaction have shown that they can describe the recent BAO observations [70–80], since they can provide an effective dark energy component with a dynamical character. Moreover, as discussed recently in [81], interacting dark energy models can explain the recent observation data without a phantom crossing scenario.

In the literature the proposed interacting models have been considered the interaction to exist for the entire cosmic history. Recently, in [82] it was found that late-time observational data support energy transfer within the dark sector. It was found that the introduction of the BAO data set combined with the Planck 2018 Cosmic Microwave Background (CMB) [83] measurements and Supernova data of the PantheonPlus [84] sample give a support to the interacting models. Thus, it is worth investigating in which period the late-time data interacting models are important for the description of the cosmos.

In this work, we adopt a different approach. We consider late-time cosmological observations and introduce an interacting dark sector model characterized by a step-like transition from a non-interacting regime to an interacting one. Specifically, we introduce a redshift-dependent coupling parameter for the interaction, with a redshift threshold parameter  $z_T$ . For  $z < z_T$  the interaction starts and supports a dynamical behaviour of dark energy, while for  $z > z_T$  the cosmological model is non-interacting. With this consideration, we are able to identify which period of cosmological history supports a transition to an interacting scenario. Furthermore, we are able to investigate whether the interaction in the dark sector is strong or weak.

We consider Supernova data, Cosmic Chronometers, and the BAO catalogue of DESI DR2, and we determine the transition redshift. We find that the data at redshifts  $z < 1$  support a strong interacting scenario with energy transfer from the dark energy to the dark matter. As a result, the model provides a larger value of the deceleration parameter at the present time, which indicates a slower expansion of the universe. Furthermore, we are able to describe the recent data without phantom

\*Electronic address: [anpaliat@phys.uoa.gr](mailto:anpaliat@phys.uoa.gr)

crossing. The structure of the paper is as follows.

In Section 2 we introduce a Friedmann–Lemaître–Robertson–Walker (FLRW) cosmological model with interacting dark sector. We introduce an interacting function which is linear to the energy density of the dark matter, where the coupling parameter that quantifies the strength of the interaction we assume that it is redshift dependent with a step transition. In Section 3 we discuss the method that we applied in this work for the statistical analysis of the theoretical models with the observational data. The results from the observational constraints are presented in Section 4, where we compare our model with the  $\Lambda$ CDM, the CPL and the interacting model with a constant coupling parameter. Finally, in Section 5 we summarize our results and draw our conclusions.

## 2. COSMOLOGICAL INTERACTING MODELS

We consider a homogeneous and isotropic universe described by the spatially flat FLRW spacetime

$$ds^2 = -dt^2 + a^2(t) (dx^2 + dy^2 + dz^2) . \quad (1)$$

where  $a(t)$  is the radius of a three-dimensional space.

Within the framework of General Relativity, the gravitational field is described by the Einstein’s field equations

$$R_{\mu\nu} - \frac{R}{2}g_{\mu\nu} = T_{\mu\nu}, \quad (2)$$

where  $T_{\mu\nu}$  describes the cosmic fluid which inherits the symmetries of the background space.

In the  $1+3$  decomposition the energy momentum tensor  $T_{\mu\nu}$  is defined as

$$T_{\mu\nu} = (\rho + p) u_\mu u_\nu + p g_{\mu\nu}, \quad (3)$$

with  $\rho$  to be the energy density,  $p = p(t)$  the pressure component.  $u^\mu$  is the fluid velocity, which we consider to be the comoving,  $u^\mu = \delta_t^\mu$ ,  $u^\mu u_\mu = -1$ , the expansion rate  $\theta(t)$  to be given by the expression  $\theta = 3H$ , where  $H = \frac{\dot{a}}{a}$  is the Hubble function.

For the line element (1) the gravitational field equations read

$$3H^2 = \rho, \quad (4)$$

$$-2\dot{H} - 3H^2 = p. \quad (5)$$

The effective equation of state parameter for the cosmological fluid is defined as  $w_{eff} = \frac{p}{\rho}$ , that is,

$$w_{eff} = -1 - \frac{2}{3} \frac{\dot{H}}{H^2}. \quad (6)$$

Hence, cosmic acceleration is described when  $w_{eff} < -\frac{1}{3}$ .

Moreover, from the Bianchi identity we recover the conservation equation for the cosmic fluid  $T^{\mu\nu}_{;\nu} = 0$ , that is,

$$\dot{\rho} + 3H(\rho + p) = 0. \quad (7)$$

We assume that the energy momentum tensor  $T_{\mu\nu}$  consists of three fluid components, the cold dark matter

$$T_{\mu\nu}^m = \rho_m u_\mu u_\nu, \quad (8)$$

the dark energy component

$$T_{\mu\nu}^{DE} = (\rho_d + p_d) u_\mu u_\nu + p_d g_{\mu\nu}. \quad (9)$$

with equation of state parameter  $w_d = \frac{p_d}{\rho_d}$ , and the baryons

$$T_{\mu\nu}^b = \rho_b u_\mu u_\nu, \quad (10)$$

where we the baryons do not interact with the rest of the fluid components

Therefore,  $\rho = \rho_m + \rho_b + \rho_d$  and  $p = p_d$ . By replacing in (7) it follows

$$(\rho_m + \rho_b + \rho_d) + 3H(\rho_m + \rho_b + \rho_d + p_d) = 0, \quad (11)$$

or equivalently,

$$\dot{\rho}_b + 3H\rho_b = 0, \quad (12)$$

$$\dot{\rho}_m + 3H\rho_m = Q, \quad (13)$$

$$\dot{\rho}_d + 3H(\rho_d + p_d) = -Q. \quad (14)$$

Here  $Q(t)$  denotes the interaction term that governs the energy exchange between dark matter and dark energy. When the two fluid do not interact  $Q(t) = 0$ . However, in interacting scenarios  $Q(t) \neq 0$ , and when  $Q(t) > 0$ , there is energy transfer from dark energy to dark matter, while for  $Q(t) < 0$  dark matter is converted into dark energy.

There is a plethora of interacting models proposed in the literature [85–90], for a review we refer the reader in [55–57].

In this work we focus on the model

$$Q_A = \alpha(z) H\rho_m,$$

where  $\alpha(z)$  is the coupling parameter that quantifies the strength of the interaction between dark energy and dark matter. This parameter is usually considered constant,  $\alpha(z) = \alpha$ . However, in this study we allow  $\alpha(z)$  to vary with redshift, introducing a step transition,

$$\alpha(z) = \frac{\alpha}{2} (1 - \tanh(\delta(z - z_T))) \quad (15)$$

where parameter  $z_T$  indicates the redshift threshold for the onset of interaction and  $\delta$  controls the sharpness of the step. We consider  $z_T > 0$  and  $\delta \gg 1$  in order the transition to the interacting sector to be fast.

Interacting models with varying coupling parameters were introduced before in [91] and applied recently for the study of the DESI DR2 data in [79]. Moreover, model where the coupling parameter change sing proposed in [76]

The existence of the step transition allows us to understand for which redshifts the interacting models become important, as also allow us to have a cosmological theory where for  $z > z_T$  the theory behaves as a non interacting model.

In the following, we focus on the case where dark energy is described by a cosmological constant,  $w_d = -1$ . For  $z < z_T$ , once the interaction is triggered, we examine deviations from  $\Lambda$ CDM.

### 3. DATA & METHODOLOGY

In the following lines, we briefly discuss the cosmological data employed in this work and the tools that we follow for the analysis of the constraints.

#### 3.1. Cosmological Data

We focus on cosmological observations with of the late-time, that is, with redshift  $z < 2.5$ . In particular we consider the Supernova data, the Cosmic Chronometers and the Baryonic Acoustic Oscillations.

##### 3.1.1. Supernova

We consider three different samples for the Supernova (SNIa) data, the PantheonPlus (PP) [84] the Union3.0 (U3) [92] and the DES-Dovekie (DESD) [93] catalogues. These catalogues provide the observable distance modulus  $\mu^{obs}$  at the redshift  $z$ . The PP sample contains 1,701 light curves corresponding to 1,550 spectroscopically supernovae events within the redshifts  $10^{-3} < z < 2.27$ . In this work we consider the PP sample without the SH0ES Cepheid calibration.

On the other hand, the U3 catalogue includes 2,087 supernova events in the same redshift range as PP, with 1,363 common events with the PP. However, the analysis of the photometric observations is different between the two catalogues.

The DESD catalogue is most recent set release of supernova data with 1820 supernova events with redshifts  $z < 1.13$  [93]. The catalogue released after the re-analysis of the five years data of the Dark Energy Survey of Type Ia supernova (DES-SN5YR), using an improved photometric calibration approach.

In a spatially flat FLRW geometry, the theoretical value of the distance modulus  $\mu^{th}$  follows from the relation  $\mu^{th} = 5 \log_{10} D_L + 25$ , where  $D_L = c(1+z) \int_0^z \frac{dz'}{H(z')}$  is the luminosity distance, and  $c$  is the speed of light.

##### 3.1.2. Cosmic Chronometers

The cosmic chronometers are passively evolving galaxies that provide us with direct measure of the Hubble

parameter. They are model independent direct measures of the Hubble parameter, leading to the Observable Hubble Dataset (OHD).

In this study we employ the 31 data presented in [94], supplemented with three additional measurements from the analysis of the DESI DR1 observations [95].

#### 3.1.3. Baryonic Acoustic Oscillations

We consider the recent release of the Dark Energy Spectroscopic Instrument (DESI DR2) baryon acoustic oscillation (BAO) observations [1–3], which provides measurements of the transverse comoving angular distance ratio,  $\frac{D_M}{r_{drag}} = \frac{D_L}{(1+z)r_{drag}}$ , the volume-averaged distance ratio,  $\frac{D_V}{r_{drag}} = \frac{(zD_H D_M^2)^{1/3}}{r_{drag}}$  and the Hubble distance ratio  $\frac{D_H}{r_d} = \frac{c}{r_{drag} H(z)}$ , at seven distinct redshifts, where  $r_{drag}$ .

### 3.2. Bayesian Analysis

For the statistical analysis we make use of the Bayesian inference framework COBAYA<sup>1</sup> [96, 97], with the use of a custom theory together with the MCMC sampler [98, 99].

For each test we consider the following combination of data SNIa&OHD&BAO, where SNIa refers to the PP, U3 or DESD catalogues.

We analyze the chains of the MCMC sampler with the GetDist library<sup>2</sup> [100], and we determine the posterior variables which maximize the likelihood  $\mathcal{L}_{\max} = \exp(-\frac{1}{2}\chi^2_{\min})$ , that is

$$\mathcal{L}_{\max} = \mathcal{L}_{SNIa} \times \mathcal{L}_{OHD} \times \mathcal{L}_{BAO},$$

that is

$$\chi^2_{\min} = \chi^2_{\min(SNIa)} + \chi^2_{\min(OHD)} + \chi^2_{\min(BAO)}.$$

#### 3.2.1. Model Comparison

We perform the analysis for the four-different models,  $\Lambda$ CDM, the Chevallier-Polarski-Linder (CPL) parametrization ( $w_0 w_a$ CDM), interacting model without threshold, and interacting model with the threshold. These models have different number of degrees of freedom, and in order to make a statistical comparison we apply the Akaike Information Criterion (AIC) [101]. For a large value of datasets.

<sup>1</sup> <https://cobaya.readthedocs.io/>

<sup>2</sup> <https://getdist.readthedocs.io/>

The AIC parameter is defined through the algebraic relation

$$AIC \simeq \chi^2_{\min} + 2\kappa, \quad (16)$$

where  $\kappa$  refers to the dimension space of the free parameters for each model.

For the  $\Lambda$ CDM the free parameters are  $\{H_0, \Omega_{m0}, r_{drag}\}$ , that is  $\kappa_{\Lambda\text{CDM}} = 3$ , for the CPL parametric dark energy model, the free parameters are five, that is,  $\kappa_{w_0 w_a \text{CDM}} = 5$ ,  $\{H_0, \Omega_{m0}, r_{drag}, w_0, w_a\}$ , and for the interacting model of our analysis without threshold ( $Q_A^0$ )  $\kappa_I = 4$ , and free parameters are  $\{H_0, \Omega_{m0}, r_{drag}, \alpha\}$ , while for the interacting models with threshold ( $Q_A$ ),  $\kappa_{IT} = 5$ , where  $\{H_0, \Omega_{m0}, r_{drag}, \alpha, z_T\}$ . As far as the parameter  $\delta$  is concerned, we assume  $\delta = 10^4$  such that the transition to the interacting era to be sharp. For the baryons we consider the value obtained by the Planck 2018 mission [83].

Akaike's scale provides information on which model offers a better fit to the data based on the value of  $\Delta AIC = AIC_A - AIC_B$ . The Akaike scale explicitly penalizes models with a large number of free parameters, thus reducing overfitting. Specifically, for  $|\Delta AIC| < 2$ , the models are equally consistent with the data, when  $2 < |\Delta AIC| < 6$ , there is weak evidence in favor of the model with the smaller AIC value; if  $6 < |\Delta AIC| < 10$ , the evidence is strong; and for  $|\Delta AIC| > 10$ , there is a clear evidence favoring for the model with the lower AIC.

#### 4. OBSERVATIONAL CONSTRAINTS

We continue our discussion with the presentation of the analysis of the MCMC chains, for the three different combinations of the datasets. The posterior variables for the interacting models  $Q_A$ ,  $Q_A^0$ , with and without the initiate mechanism are presented in Table I. Moreover, in Tables II and III we provide the statistical comparison of the two interacting models  $Q_A$  and  $Q_A^0$ , with the  $\Lambda$ CDM and the CPL models.

In Figs. 1 and 2 we present the contours for the confidence space of the free parameters for the  $Q_A$  and  $Q_A^0$  models respectively.

##### 4.1. PP&OHD&BAO

For the first combination data, where we consider the PP catalogue for the SNIa, from the interacting model  $Q_A$  we find the posterior variables  $H_0 = 68.2^{+1.7}_{-1.7}$ ,  $\Omega_{m0} = 0.334^{+0.029}_{-0.074}$ ,  $r_{drag} = 146.9^{+3.1}_{-3.6}$ ,  $\alpha = 1.55^{+0.55}_{-1.4}$  and  $z_T < 0.624$ , while for the interaction without the threshold, i.e.  $Q_A^0$ , we derive  $H_0 = 68.0^{+1.9}_{-1.6}$ ,  $\Omega_{m0} = 0.300^{+0.009}_{-0.035}$ ,  $r_{drag} = 147.2^{+3.1}_{-4.1}$ ,  $\alpha = 0.203^{+0.021}_{-0.18}$ .

The comparison of the statistical parameters shows that model  $Q_A$  and CPL fit the data with the same way,

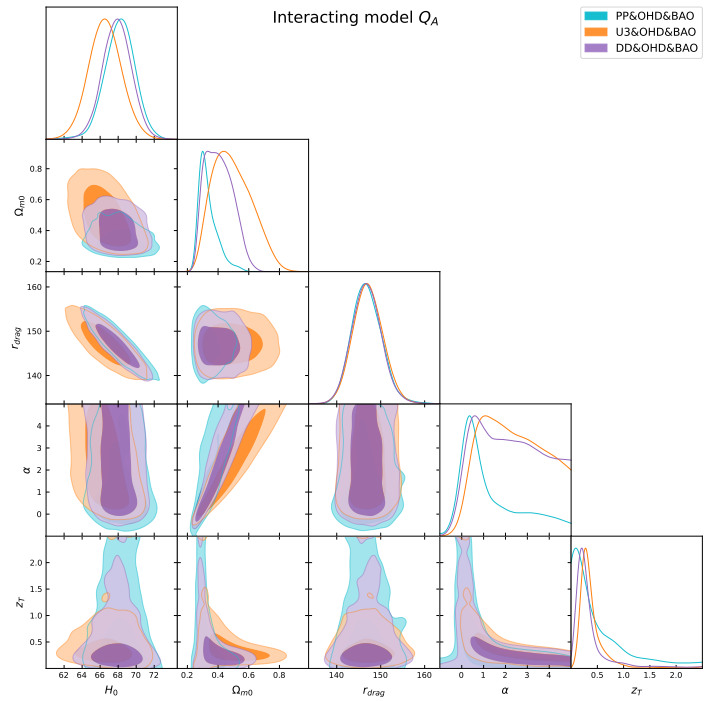


Figure 1: Confidence space for the posterior parameters  $\{H_0, \Omega_{m0}, r_{drag}, \alpha, z_T\}$  for the interacting model  $Q_A$ .

$\chi^2_{\min}(Q_A) - \chi^2_{\min}(\text{CPL}) \simeq +0.01$  and better in comparison to the  $\Lambda$ CDM and  $Q_A^0$  models, that is,  $\chi^2_{\min}(Q_A) - \chi^2_{\min}(\Lambda) \simeq -3.37$ ,  $\chi^2_{\min}(Q_A^0) - \chi^2_{\min}(\Lambda) \simeq -1.86$  and  $\chi^2_{\min}(Q_A^0) - \chi^2_{\min}(\text{CPL}) \simeq +1.52$ . However, due to the different number of degrees of freedom, the four models are statistically equivalent.

##### 4.2. U3&OHD&BAO

We consider the U3 catalogue for the SNIa. For the interacting model  $Q_A$  we find the posterior variables  $H_0 = 66.6^{+1.8}_{-1.8}$ ,  $\Omega_{m0} = 0.490^{+0.10}_{-0.15}$ ,  $r_{drag} = 147.1^{+3.4}_{-3.4}$ ,  $\alpha = 2.4^{+1.1}_{-1.9}$  and  $z_T = 0.400^{+0.021}_{-0.23}$ , while for  $Q_A^0$  it follows  $H_0 = 67.1^{+2.4}_{-1.6}$ ,  $\Omega_{m0} = 0.337^{+0.002}_{-0.066}$ ,  $r_{drag} = 147.7^{+3.2}_{-4.2}$ ,  $\alpha = 0.324^{+0.011}_{-0.25}$ .

From Tables II and III it follows  $\chi^2_{\min}(Q_A) - \chi^2_{\min}(\text{CPL}) \simeq +0.34$ ,  $\chi^2_{\min}(Q_A) - \chi^2_{\min}(\Lambda) \simeq -7.9$ ,  $\chi^2_{\min}(Q_A^0) - \chi^2_{\min}(\text{CPL}) \simeq +5.54$  and  $\chi^2_{\min}(Q_A^0) - \chi^2_{\min}(\Lambda) \simeq -2.7$ .

Thus,  $Q_A$  and the CPL model fit the data in the same way, while in comparison to the  $\Lambda$ CDM and the  $Q_A^0$ , there is a weak evidence in favor to the  $Q_A$ . However,

##### 4.3. DD&OHD&BAO

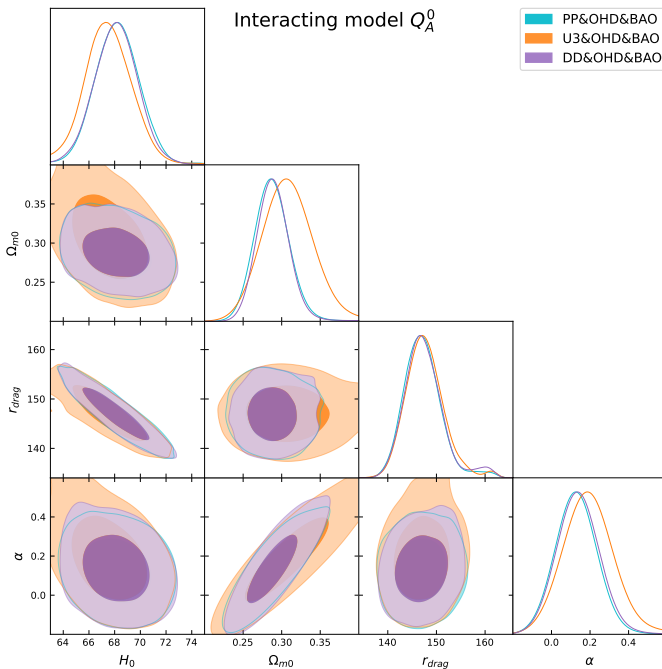
Finally, the application of the DD sample for the SNIa, for model  $Q_A$  we derive the posterior variables  $H_0 =$

Table I: Posterior variables for the interacting models as given by the analysis of the MCMC chains.

Data Set	$H_0$	$\Omega_{m0}$	$r_{drag}$	$\alpha$	$z_T$
<b>Model <math>Q_A</math></b>					
<b>PP&amp;OHD&amp;BAO</b>	$68.2^{+1.7}_{-1.7}$	$0.334^{+0.029}_{-0.074}$	$146.9^{+3.1}_{-3.6}$	$1.55^{+0.55}_{-1.4}$	$< 0.624$
<b>U3&amp;OHD&amp;BAO</b>	$66.6^{+1.8}_{-1.8}$	$0.490^{+0.10}_{-0.15}$	$147.1^{+3.4}_{-3.4}$	$2.4^{+1.1}_{-1.9}$	$0.400^{+0.021}_{-0.23}$
<b>DD&amp;OHD&amp;BAO</b>	$67.9^{+1.6}_{-1.6}$	$0.406^{+0.071}_{-0.11}$	$146.8^{+3.4}_{-3.4}$	$2.2^{+1.0}_{-2.2}$	$0.371^{+0.028}_{-0.26}$
<b>Model <math>Q_A^0</math></b>					
<b>PP&amp;OHD&amp;BAO</b>	$68.0^{+1.9}_{-1.6}$	$0.300^{+0.009}_{-0.035}$	$147.2^{+3.1}_{-4.1}$	$0.203^{+0.021}_{-0.18}$	—
<b>U3&amp;OHD&amp;BAO</b>	$67.1^{+2.4}_{-1.6}$	$0.337^{+0.002}_{-0.066}$	$147.7^{+3.2}_{-4.2}$	$0.324^{+0.011}_{-0.25}$	—
<b>DD&amp;OHD&amp;BAO</b>	$67.9^{+1.9}_{-1.6}$	$0.301^{+0.007}_{-0.034}$	$147.6^{+3.0}_{-4.3}$	$0.229^{+0.015}_{-0.19}$	—

Table II: Statistical comparison of the interacting model with with the initiate mechanism with respect to the  $\Lambda$ CDM and the CPL.

Data Set	Reference Model	Base Model	$\Delta\chi^2_{\min}$	$\Delta\text{AIC}$	Akaike's Scale
PP&OHD&BAO	$\Lambda$ CDM	$Q_A$	-3.37	+0.63	Inconclusive
PP&OHD&BAO	CPL	$Q_A$	+0.01	+0.01	Inconclusive
U3&OHD&BAO	$\Lambda$ CDM	$Q_A$	-7.9	-3.9	Weak Evidence in favor of $Q_A$
U3&OHD&BAO	CPL	$Q_A$	+0.34	+0.34	Inconclusive
DD&OHD&BAO	$\Lambda$ CDM	$Q_A$	-6.42	-2.42	Weak Evidence in favor of $Q_A$
DD&OHD&BAO	CPL	$Q_A$	-1.65	-1.65	Inconclusive

Figure 2: Confidence space for the posterior parameters  $\{H_0, \Omega_{m0}, r_{drag}, \alpha\}$  for the interacting model  $Q_A^0$ .

$67.9^{+1.6}_{-1.6}$ ,  $\Omega_{m0} = 0.406^{+0.071}_{-0.11}$ ,  $r_{drag} = 146.8^{+3.4}_{-3.4}$ ,  $\alpha = 2.2^{+1.0}_{-2.2}$  and  $z_T = 0.371^{+0.028}_{-0.26}$ , while for  $Q_A^0$  we calculate  $H_0 = 67.9^{+1.9}_{-1.6}$ ,  $\Omega_{m0} = 0.301^{+0.007}_{-0.034}$ ,  $r_{drag} = 147.6^{+3.0}_{-4.3}$ ,  $\alpha = 0.229^{+0.015}_{-0.19}$ .

Moreover, Tables II and III reveal,  $\chi^2_{\min}(Q_A) - \chi^2_{\min}(\text{CPL}) \simeq -1.65$ ,  $\chi^2_{\min}(Q_A) - \chi^2_{\min}(\Lambda) \simeq -6.42$ ,  $\chi^2_{\min}(Q_A^0) - \chi^2_{\min}(\text{CPL}) \simeq +2.57$  and  $\chi^2_{\min}(Q_A^0) - \chi^2_{\min}(\Lambda) \simeq -2.2$ .

Therefore, model  $Q_A$  fits the data in a better way than the rest of the models, and its comparison to the  $\Lambda$ CDM and the  $Q_A^0$  the data provide a weak evidence in favor to the  $Q_A$ . Nevertheless, Akaike's scale indicate that  $Q_A$  and CPL models are statistically equivalent.

#### 4.4. Discussion

The analysis of the observational constraints for the interacting model  $Q_A$  with the three different data sets, reveal that the transition to a interacting sector is at small redshifts  $z < 0.5$ . Moreover, the interacting coupling parameter  $\alpha$  for the  $Q_A$  is found to be approximately eight times larger than the coupling parameter for the model  $Q_A$ , from where we infer that the late-time observational data, with  $z < 0.5$ , support a strong interacting scenario.

In Figs. 3, 4 and 5 we present the qualitative evolution of the energy densities for the dark matter  $\Omega_m(z)$ , the dark energy  $\Omega_{DE}(z)$ , and the deceleration parameters  $q(z)$  for the best-fit parameters given in Table I for the three different data sets and we compare them with the  $\Lambda$ CDM and the CPL parametrization.

Because of the strong positive interacting coupling parameter for model  $Q_A$ , the data suggests a transition to a slower acceleration rate at the present time in comparison to the  $\Lambda$ CDM, which is in agreement with the

Table III: Statistical comparsion of the interacting model without the initiate mechanism with respect to the  $\Lambda$ CDM and the CPL.

Data Set	Reference Model	Base Model	$\Delta\chi^2_{\min}$	$\Delta\text{AIC}$	Akaike's Scale
PP&OHD&BAO	$\Lambda$ CDM	$Q_A^0$	-1.86	+0.14	Inconclusive
PP&OHD&BAO	CPL	$Q_A^0$	+1.52	-0.48	Inconclusive
U3&OHD&BAO	$\Lambda$ CDM	$Q_A^0$	-2.7	+0.7	Inconclusive
U3&OHD&BAO	CPL	$Q_A^0$	+5.54	+3.54	Weak Evidence in favor of CPL
DD&OHD&BAO	$\Lambda$ CDM	$Q_A^0$	-2.2	-0.2	Inconclusive
DD&OHD&BAO	CPL	$Q_A^0$	+2.57	-0.57	Inconclusive

behaviour provided by the CPL model. On the other hand, for  $z > 0.5$ , the interacting model  $Q_A$  suggests a higher acceleration rate for the universe, while for large values of redshift, due to the different values of the  $\Omega_m$  at the transition point  $z_T$ . Recall that for  $z > z_T$ ,  $Q_A$  and  $\Lambda$ CDM are identical.

## 5. CONCLUSIONS

Models with interaction in the dark sector of the universe provide a simple mechanism for the description of the dynamical character of dark energy, and it has been shown that they can challenge the  $\Lambda$ CDM model in the description of late-time observational data. In this work, we considered a phenomenological interacting dark sector with a redshift threshold for the onset of the interacting term. This consideration allowed us to understand during which period of cosmic evolution the interacting terms appear and play an contribute in the phase-transition of the dark sector.

In particular, we considered an extension of the  $\Lambda$ CDM model with an interacting term linear in the dark matter component and a step potential that depends on the transition redshift  $z_T$ . For  $z < z_T$  the interaction appears, while for  $z > z_T$  the model behaves as  $\Lambda$ CDM. We tested this model using recent cosmological data, specifically cosmic chronometers, BAO data, and SNIa data from the PP, U3, and DD samples. For the three different combinations of data sets, we determined the posterior space of the free parameters of the model under consideration. We performed the same tests for the same interacting model without the onset mechanism, for  $\Lambda$ CDM, and for the CPL parametrized dark energy model.

We found that the interacting model with the onset mechanism fits the data better than the simple interacting model. The data show a weak preference for our model compared to  $\Lambda$ CDM or the interacting model with a constant coupling parameter. Nevertheless, our model is statistically equivalent to the CPL model. Our interacting model and the CPL model share the same number of free parameters and fit the three data sets in a similar way. Specifically, for PP&OHD&BAO we find  $\chi^2_{\min}(Q_A) - \chi^2_{\min}(\text{CPL}) \simeq +0.01$ , for U3&OHD&BAO

we derive  $\chi^2_{\min}(Q_A) - \chi^2_{\min}(\text{CPL}) \simeq +0.34$ , while for the combined data set DD&OHD&BAO the analysis provides  $\chi^2_{\min}(Q_A) - \chi^2_{\min}(\text{CPL}) \simeq -1.65$ . Importantly, our interacting model is able to reproduce the observational data at the same level as the CPL model without requiring a phantom crossing of the dark energy equation of state.

Furthermore, we found that the transition point  $z_T$  for the PP&OHD&BAO data set is  $z_T < 0.624$ , for U3&OHD&BAO the transition is at  $z_T = 0.400^{+0.021}_{-0.23}$ , and for DD&OHD&BAO the transition point is at  $z_T = 0.371^{+0.028}_{-0.26}$ . All three data sets favor a large and positive coupling parameter, indicating a strong energy transfer from dark energy to dark matter at late times. As a result, the deceleration parameter for  $z < z_T$  increases, such that the expansion of the universe proceeds at a smaller rate.

In this work we have not considered early universe observational data. However, from the results of [82] it is known that the late-time data support an interacting model, while early-data supports  $\Lambda$ CDM, and because for  $z > z_T$  our model behaves identical with the  $\Lambda$ CDM we expect that our model fits the early-time data in a similar way to the  $\Lambda$ CDM.

The exact mechanism for the energy transfer between dark energy and dark matter is not known. However, we can refer to the dark sector as a single fluid with two different components. In this one fluid description, the energy transfer mechanism is effective and can be interpreted as a phase transition of the fluid. Within this framework, the onset mechanism that triggers the phase transition can be easily introduced. Such behaviour is provided by the hameleon mechanism [102] and in general within the symmetron cosmology [103].

In future work, we plan to investigate the introduction of the step mechanism within a theoretical framework.

## Acknowledgments

AP acknowledges the support from FONDECYT Grant 1240514 and from VRIDT through Resolución VRIDT No. 096/2022 and Resolución VRIDT No. 098/2022.

- 
- [1] M. Abdul Karim et al. (DESI) (2025), 2503.14739.
- [2] M. Abdul Karim et al. (DESI) (2025), 2503.14738.
- [3] K. Lodha et al. (DESI) (2025), 2503.14743.
- [4] S. Arora, A. De Felice, and S. Mukohiyama, Phys. Rev. D **112**, 123518 (2025), 2508.03784.
- [5] D. A. Kessler, L. A. Escamilla, S. Pan, and E. Di Valentino, *One-parameter dynamical dark energy: Hints for oscillations* (2025), 2504.00776.
- [6] X. Zhang, Y.-H. Xu, and Y. Sang, Commun. Theor. Phys. **78**, 035404 (2026), 2511.02220.
- [7] A. Paliathanasis, Phys. Dark Univ. **48**, 101956 (2025), 2502.16221.
- [8] R. Nagpal, H. Chaudhary, H. Gupta, and S. K. J. Pacif, JHEAp **47**, 100396 (2025).
- [9] A. N. Ormondroyd, W. J. Handley, M. P. Hobson, and A. N. Lasenby (2025), 2503.17342.
- [10] C. You, D. Wang, and T. Yang, Phys. Rev. D **112**, 043503 (2025), 2504.00985.
- [11] M. Scherer, M. A. Sabogal, R. C. Nunes, and A. De Felice, Phys. Rev. D **112**, 043513 (2025), 2504.20664.
- [12] S. Paradiso, G. McGee, and W. J. Percival, JCAP **10**, 021 (2024), 2403.02120.
- [13] A. G. Adame et al. (DESI), JCAP **02**, 021 (2025), 2404.03002.
- [14] C.-G. Park, J. de Cruz Pérez, and B. Ratra, Phys. Rev. D **110**, 123533 (2024), 2405.00502.
- [15] C.-G. Park and B. Ratra, Int. J. Mod. Phys. D **34**, 2550061 (2025), 2501.03480.
- [16] C.-G. Park, J. de Cruz Pérez, and B. Ratra, Int. J. Mod. Phys. D **34**, 2550058 (2025), 2410.13627.
- [17] A. C. Alfano and O. Luongo, *Cosmic distance duality after DESI 2024 data release and dark energy evolution* (2025), 2501.15233.
- [18] Y. Carloni, O. Luongo, and M. Muccino, Phys. Rev. D **111**, 023512 (2025), 2404.12068.
- [19] G. Alestas, M. Caldarola, I. Ocampo, S. Nesseris, and S. Tsujikawa, *DESI constraints on two-field quintessence with exponential potentials* (2025), 2510.21627.
- [20] S. Sánchez López, A. Karam, and D. K. Hazra, *Non-Minimally Coupled Quintessence in Light of DESI* (2025), 2510.14941.
- [21] A. Pourtsidou, *Exponential quintessence with momentum coupling to dark matter* (2025), 2509.15091.
- [22] Y. Yang, Q. Wang, X. Ren, E. N. Saridakis, and Y.-F. Cai, Astrophys. J. **988**, 123 (2025), 2504.06784.
- [23] Z. Lu and T. Simon, *A new multiprobe analysis of modified gravity and evolving dark energy* (2025), 2511.10616.
- [24] S. Feng, Y. Gong, X. Liu, J.-H. Yan, and X. Chen, *Constraining and Comparing the Dynamical Dark Energy and f(R) Modified Gravity Models with Cosmological Distance Measurements* (2025), 2510.23105.
- [25] P. Karmakar and S. Haridasu (2025), 2509.07976.
- [26] A. Samaddar and S. S. Singh, Eur. Phys. J. C **85**, 1357 (2025), 2507.14251.
- [27] O. H. E. Philcox, E. Silverstein, and G. Torroba (2025), 2507.00115.
- [28] A. Paliathanasis, Phys. Dark Univ. **49**, 101993 (2025), 2504.11132.
- [29] S. D. Odintsov, V. K. Oikonomou, and G. S. Sharov, JHEAp **50**, 100471 (2026), 2506.02245.
- [30] F. Plaza and L. Kraiselburg, Phys. Rev. D **112**, 023554 (2025), 2504.05432.
- [31] S. D’Onofrio, S. Odintsov, and T. Schiavone (2025), 2511.06924.
- [32] J. A. Nájera, I. Banik, H. Desmond, and V. Kalaitzidis (2025), 2510.20964.
- [33] M. W. Hossain and A. Maqsood, Phys. Rev. D **112**, 083504 (2025), 2502.19274.
- [34] A. J. Shajib and J. A. Frieman, Phys. Rev. D **112**, 063508 (2025), 2502.06929.
- [35] L. A. Anchordoqui, I. Antoniadis, and D. Lust, Phys. Lett. B **868**, 139632 (2025), 2503.19428.
- [36] A. Paliathanasis, *Observational Constraints on Scalar Field–Matter Interaction in Weyl Integrable Spacetime* (2025), 2506.16223.
- [37] A. Paliathanasis, T. Mengoni, G. Leon, and O. Luongo (2025), 2512.00558.
- [38] Y. Cai, X. Ren, T. Qiu, M. Li, and X. Zhang, *The Quintom theory of dark energy after DESI DR2* (2025), 2505.24732.
- [39] G. Ye and Y. Cai, Phys. Rev. D **112**, L121301 (2025).
- [40] M. W. Toomey, E. Hughes, M. M. Ivanov, and J. M. Sullivan (2025), 2511.23463.
- [41] C. Zheng, W. Liu, Z. Zhan, and W. Fang, Res. Astron. Astrophys. **25**, 125015 (2025), 2509.13804.
- [42] X. Shen, B. Xu, K. Zhang, X. Fu, L. Ren, and Z. Zhang, Eur. Phys. J. C **85**, 992 (2025).
- [43] S. Hussain, Q. Wu, and T. Zhu (2025), 2509.09202.
- [44] M. Yadav, A. Dixit, A. Pradhan, and M. S. Barak, JHEAp **49**, 100453 (2026), 2509.26049.
- [45] A. Paliathanasis, JCAP **09**, 067 (2025), 2503.20896.
- [46] A. Paliathanasis, G. Leon, Y. Leyva, G. G. Luciano, and A. Abebe (2025), 2508.20644.
- [47] M. Yadav, A. Dixit, M. S. Barak, and A. Pradhan, JHEAp **50**, 100514 (2026).
- [48] G. G. Luciano, A. Paliathanasis, and E. N. Saridakis, JHEAp **49**, 100427 (2026), 2506.03019.
- [49] O. Luongo and M. Muccino, Astron. Astrophys. **690**, A40 (2024), 2404.07070.
- [50] P. Thanankullaphong, P. Sahoo, P. H. Puttasiddappa, and N. Roy, *Quintom Dark Energy: Future Attractor and Phantom Crossing in Light of DESI DR2 Observation* (2026), 2601.02284.
- [51] B. Wang, E. Abdalla, F. Atrio-Barandela, and D. Pavon, Rept. Prog. Phys. **79**, 096901 (2016), 1603.08299.
- [52] G. R. Farrar and P. J. E. Peebles, Astrophys. J. **604**, 1 (2004), astro-ph/0307316.
- [53] M. Lucca, Phys. Dark Univ. **34**, 100899 (2021), 2105.09249.
- [54] M. Lucca and D. C. Hooper, Phys. Rev. D **102**, 123502 (2020), 2002.06127.
- [55] M. van der Westhuizen, A. Abebe, and E. Di Valentino, *I. Linear Interacting Dark Energy: Analytical Solutions and Theoretical Pathologies* (2025), 2509.04495.
- [56] M. van der Westhuizen, A. Abebe, and E. Di Valentino, *II. Non-Linear Interacting Dark Energy: Analytical Solutions and Theoretical Pathologies* (2025), 2509.04494.
- [57] M. van der Westhuizen, A. Abebe, and E. Di Valentino, *III. Interacting Dark Energy: Summary of Models, Pathologies, and Constraints* (2025), 2509.04496.

- [58] W. Giarè, M. A. Sabogal, R. C. Nunes, and E. Di Valentino, Phys. Rev. Lett. **133**, 251003 (2024), 2404.15232.
- [59] W. Giarè, Y. Zhai, S. Pan, E. Di Valentino, R. C. Nunes, and C. van de Bruck, Phys. Rev. D **110**, 063527 (2024), 2404.02110.
- [60] D. Benisty, S. Pan, D. Staicova, E. Di Valentino, and R. C. Nunes, Astron. Astrophys. **688**, A156 (2024), 2403.00056.
- [61] G. Okeng'o, N. Mhlahlo, and R. Maartens, Eur. Phys. J. C **84**, 569 (2024), 2403.01986.
- [62] J. Valiviita, E. Majerotto, and R. Maartens, JCAP **07**, 020 (2008), 0804.0232.
- [63] G. Caldera-Cabral, R. Maartens, and L. A. Urena-Lopez, Phys. Rev. D **79**, 063518 (2009), 0812.1827.
- [64] Y. Zhai, W. Giarè, C. van de Bruck, E. Di Valentino, O. Mena, and R. C. Nunes, JCAP **07**, 032 (2023), 2303.08201.
- [65] S. Pan, W. Yang, E. Di Valentino, E. N. Saridakis, and S. Chakraborty, Phys. Rev. D **100**, 103520 (2019), 1907.07540.
- [66] S. Pan, G. S. Sharov, and W. Yang, Phys. Rev. D **101**, 103533 (2020), 2001.03120.
- [67] W. Yang, S. Vagnozzi, E. Di Valentino, R. C. Nunes, S. Pan, and D. F. Mota, JCAP **07**, 037 (2019), 1905.08286.
- [68] A. Paliathanasis, S. Pan, and W. Yang, Int. J. Mod. Phys. D **28**, 1950161 (2019), 1903.02370.
- [69] W. Yang, N. Banerjee, A. Paliathanasis, and S. Pan, Phys. Dark Univ. **26**, 100383 (2019), 1812.06854.
- [70] Z. Zhu, Q. Jiang, Y. Liu, P. Wu, and N. Liang (2025), 2511.16032.
- [71] Y.-M. Zhang, T.-N. Li, G.-H. Du, S.-H. Zhou, L.-Y. Gao, J.-F. Zhang, and X. Zhang (2025), 2510.12627.
- [72] T.-N. Li, G.-H. Du, Y.-H. Li, Y. Li, J.-L. Ling, J.-F. Zhang, and X. Zhang (2025), 2510.11363.
- [73] V. Petri, V. Marra, and R. von Marttens (2025), 2508.17955.
- [74] Y.-H. Li and X. Zhang (2025), 2506.18477.
- [75] S. Pan, S. Paul, E. N. Saridakis, and W. Yang (2025), 2504.00994.
- [76] E. Silva, M. A. Sabogal, M. Scherer, R. C. Nunes, E. Di Valentino, and S. Kumar, Phys. Rev. D **111**, 123511 (2025), 2503.23225.
- [77] R. Shah, P. Mukherjee, and S. Pal, Mon. Not. Roy. Astron. Soc. **542**, 2936 (2025), 2503.21652.
- [78] L. Feng, T.-N. Li, G.-H. Du, J.-F. Zhang, and X. Zhang, Phys. Dark Univ. **48**, 101935 (2025), 2503.10423.
- [79] W. Yang, S. Zhang, O. Mena, S. Pan, and E. Di Valentino, *Dark Energy Is Not That Into You: Variable Couplings after DESI DR2 BAO* (2025), 2508.19109.
- [80] M. van der Westhuizen, D. Figueuelo, R. Thubisi, S. Sahlu, A. Abebe, and A. Paliathanasis, Phys. Dark Univ. **50**, 102107 (2025), 2505.23306.
- [81] S. L. Guedezounme, B. R. Dinda, and R. Maartens (2025), 2507.18274.
- [82] Y. Zhai, M. de Cesare, C. van de Bruck, E. Di Valentino, and E. Wilson-Ewing, JCAP **11**, 010 (2025), 2503.15659.
- [83] N. Aghanim et al. (Planck), Astron. Astrophys. **641**, A6 (2020), [Erratum: Astron. Astrophys. 652, C4 (2021)], 1807.06209.
- [84] D. Brout et al., Astrophys. J. **938**, 110 (2022), 2202.04077.
- [85] N. A. Koshelev, Gen. Rel. Grav. **43**, 1309 (2011), 0912.0120.
- [86] G. Mangano, G. Miele, and V. Pettorino, Mod. Phys. Lett. A **18**, 831 (2003), astro-ph/0212518.
- [87] D. G. A. Duniya, D. Bertacca, and R. Maartens, Phys. Rev. D **91**, 063530 (2015), 1502.06424.
- [88] E. Majerotto, J. Valiviita, and R. Maartens, Mon. Not. Roy. Astron. Soc. **402**, 2344 (2010), 0907.4981.
- [89] E. Majerotto, J. Valiviita, and R. Maartens, Nucl. Phys. B Proc. Suppl. **194**, 260 (2009).
- [90] A. Paliathanasis, K. Duffy, A. Halder, and A. Abebe, Phys. Dark Univ. **47**, 101750 (2025), 2409.05348.
- [91] W. Yang, O. Mena, S. Pan, and E. Di Valentino, Phys. Rev. D **100**, 083509 (2019), 1906.11697.
- [92] D. Rubin et al., arXiv preprint arXiv:2311.12098 (2023).
- [93] B. Popovic et al. (DES) (2025), 2511.07517.
- [94] M. Moresco et al., The Astrophysical Journal **898**, 82 (2020).
- [95] S. I. Loubser (2025), 2511.02730.
- [96] J. Torrado and A. Lewis, Astrophysics Source Code Library, (2019), ascl:1910.019.
- [97] J. Torrado and A. Lewis, JCAP **05**, 057 (2021), 2005.05290.
- [98] A. Lewis and S. Bridle, Phys. Rev. D **66**, 103511 (2002), astro-ph/0205436.
- [99] A. Lewis, Phys. Rev. D **87**, 103529 (2013), 1304.4473.
- [100] A. Lewis, JCAP **08**, 025 (2025), 1910.13970.
- [101] H. Akaike, IEEE Trans. Automatic Control **19**, 716 (1974).
- [102] J. Khoury and A. Weltman, Phys. Rev. D **69**, 044026 (2004), astro-ph/0309411.
- [103] K. Hinterbichler, J. Khoury, A. Levy, and A. Matas, Phys. Rev. D **84**, 103521 (2011), 1107.2112.

## PP&amp;OHD&amp;BAO

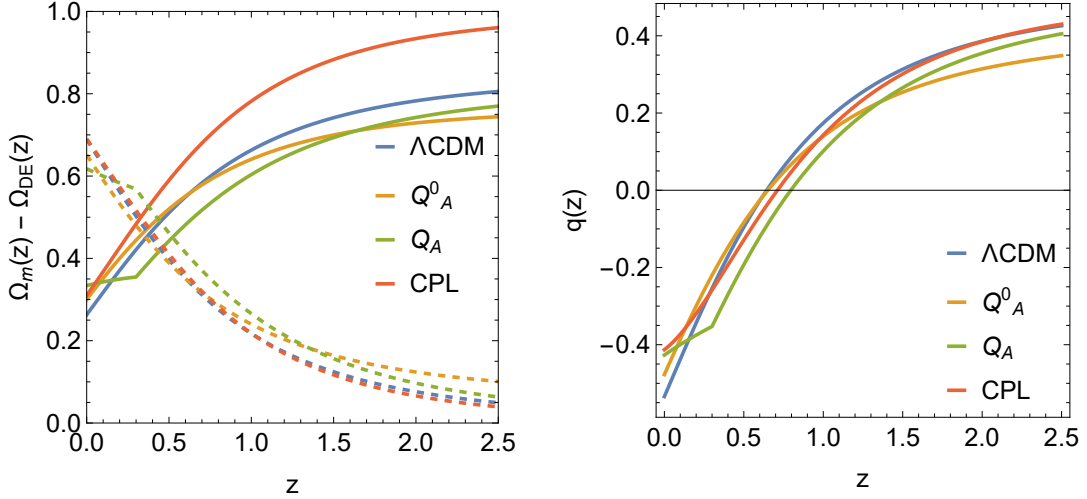


Figure 3: PP&OHD&BAO: Left Fig: Qualitative evolution of the  $\Omega_m(z)$  (solid lines) and  $\Omega_{DE}(z)$  (dashed lines) for the  $\Lambda$ CDM, the  $Q_A^0$  and  $Q_A$  interacting models. Right Fig: Qualitative evolution of the deceleration parameter  $q(z) = \frac{1}{2}(1 + 3w_{tot}(z))$ . Plots are for the best-fit parameters. Blue lines are for the  $\Lambda$ CDM, orange and green lines are for the  $Q_A^0$  and  $Q_A$  interacting models respectively, red lines are for the CPL parametrization.

## U3&amp;OHD&amp;BAO

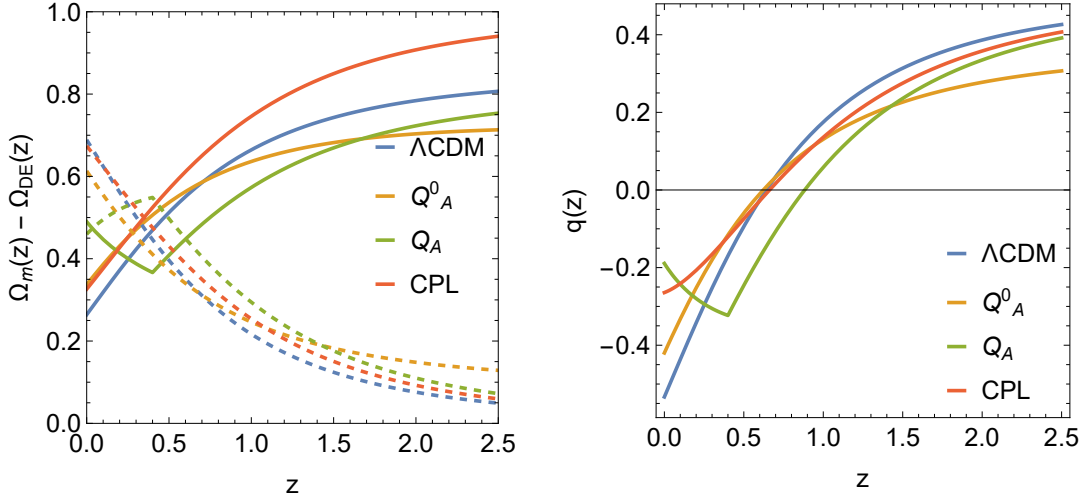


Figure 4: U3&OHD&BAO: Left Fig: Qualitative evolution of the  $\Omega_m(z)$  (solid lines) and  $\Omega_{DE}(z)$  (dashed lines) for the  $\Lambda$ CDM, the  $Q_A^0$  and  $Q_A$  interacting models. Right Fig: Qualitative evolution of the deceleration parameter  $q(z) = \frac{1}{2}(1 + 3w_{tot}(z))$ . Plots are for the best-fit parameters. Blue lines are for the  $\Lambda$ CDM, orange and green lines are for the  $Q_A^0$  and  $Q_A$  interacting models respectively, red lines are for the CPL parametrization.

## DD&amp;OHD&amp;BAO

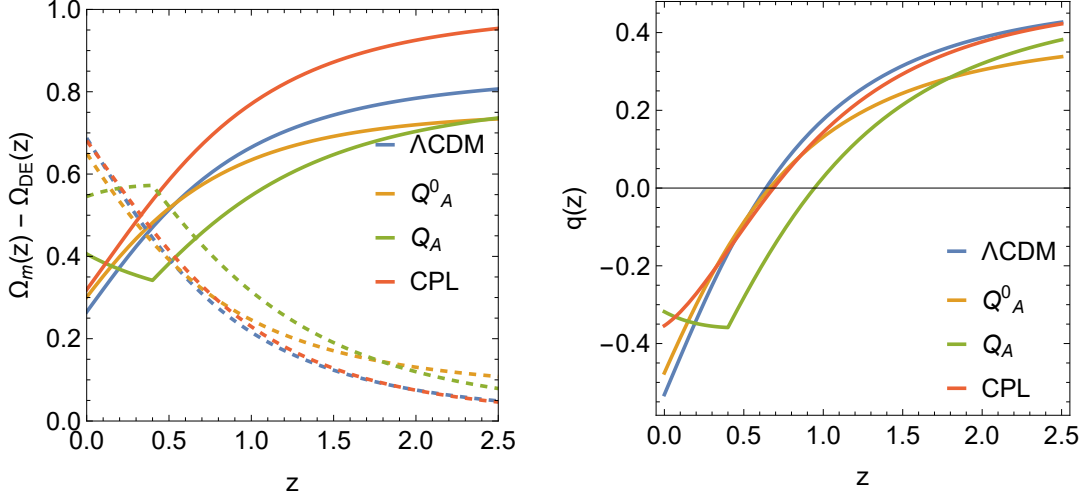


Figure 5: DD&OHD&BAO: Left Fig: Qualitative evolution of the  $\Omega_m(z)$  (solid lines) and  $\Omega_{DE}(z)$  (dashed lines) for the  $\Lambda$ CDM, the  $Q_A^0$  and  $Q_A$  interacting models. Right Fig: Qualitative evolution of the deceleration parameter  $q(z) = \frac{1}{2}(1 + 3w_{tot}(z))$ . Plots are for the best-fit parameters. Blue lines are for the  $\Lambda$ CDM, orange and green lines are for the  $Q_A^0$  and  $Q_A$  interacting models respectively, red lines are for the CPL parametrization.